Proceedings of 4th CIRP International Conference on High Performance Cutting, 2010

Modeling Dynamics of Parallel Turning Operations

Erdem Ozturk and Erhan Budak
Manufacturing Research Laboratory, Sabanci University, Istanbul, Turkey
erdemoz@su.sabanciuniv.edu, ebudak@sabanciuniv.edu

Abstract:
Parallel turning operations are advantageous in terms of productivity since there are more than one cutting tools in operation. However, the dynamic interaction between these parallel tools may create additional stability problems and the advantage of parallel turning may not be utilized to full extent. For that reason, dynamics and stability of parallel turning processes need to be modeled. In this paper, dynamics of two different parallel turning operations where two turning tools cut a common workpiece are modeled. In the first case, the tools are directly coupled to each other whereas in the other case the coupling occurs through the vibration waves left on the workpiece. For these two cases, stability models in frequency and time domain have been developed. The frequency and time-domain solution results are compared and a reasonable agreement is observed. The predicted stability limits are also compared with experimental results where good agreement is demonstrated.

Keywords: Parallel turning, chatter vibrations, cutting stability

1. Introduction

In parallel turning operations more than one turning tool cut a common workpiece simultaneously. Due to the parallel working tools, these processes have potential for increased productivity. However, dynamic interactions among the tools may result in additional stability problems and the advantage of using parallel processes may be compromised.

The stability of single tool turning processes has been studied in detail by many researchers. The initial works about orthogonal turning stability belong to Tobias and Fishwick [1], and Tlusty and Polacek [2]. They demonstrated regenerative effect between dynamic cutting forces and dynamic displacements which results in chatter vibrations. Moreover, they predicted the stability limits in order to eliminate these vibrations. Later, Tlusty and Ismail [3] performed time domain simulations and acquired more accurate results for stability limits. Moufki et. al [4] applied thermo-mechanical model of cutting to the one dimensional stability formulation. Chen et al. [5] and Vela-Martinez, et al. [6] added the workpiece dynamics in the stability formulations. Rao et al. [7] extended the stability formulation to 3D for three-dimensional oblique turning operations. They included the cross-coupling between radial and axial vibrations in the force model. Similarly, Ozlu and Budak [8] formulated the stability considering the displacements of tool and workpiece in radial and axial directions. Moreover, they showed the effect of nose radius on the stability limits. In another study, Ozlu and Budak [9] showed that when inclination angle or nose radius exists on the tool, multi-dimensional solution is needed since the one dimensional stability formulation [2] fails to represent the dynamics of the process accurately.

Although there are substantial amount of work done on chatter stability for standard turning operations, there are only a few studies on parallel turning process stability. Lazoglu et al. [10] formulated a parallel turning process in time domain where each tool cuts a different surface. There is no direct interaction between the tools in the presented case; the dynamic coupling between the tools occurs through the flexible workpiece. By simulations, they showed that parallel working tools decrease the stability limits of each other. Later, Ozdoganlar and Endres [11] developed a parallel turning process on a modified vertical milling machine where they cut different surfaces. Dynamic interaction between the tools is achieved using an angle plate and the workpiece is rigid. The analytical solution provided is valid for symmetric systems. They validated the developed formulation through experimental results.

In this paper, dynamics of two different parallel turning operations are modeled. In the first case, a specially designed tool holder which can hold two cutting tools is used on a standard turning center. There is direct dynamic coupling between the tools since they are on the same turret location. In the second case, the turning tools are clamped on independent turrets on a parallel turning center. In this case, there is no direct dynamic coupling between the tools, but they dynamically interact through the workpiece. The formulations for both cases are presented in the next section. In section 3, the procedure developed for generation of stability diagrams is explained. The stability limit predictions of the presented model are demonstrated for different cases and the simulation results are compared by experimental data in section 4.

2. Formulating Dynamics of Parallel Turning

Dynamics of two different parallel turning operations are modeled in this section. In the first case, two turning tools are clamped on a specially designed tool holder on a standard turning centre as shown in Figure 1(a). The movements of the tools are dependent on each other since they are on the same turret; but they cut different surfaces on the workpiece. In the second case, two turning tools are clamped on different tool holders on different turrets on a parallel machining centre as presented in Figure 1(b). Although the turrets can move independently, they cut the same surface on the workpiece. The dynamics of each case is analyzed in the following subsections.

(a) (b)

Figure 1: Parallel turning cases (a) two turning tools on the same turret (b) two turning tools on different turrets

2.1 Two turning tools on the same turret

A parallel turning process with two turning tools on the same turret machining different surfaces is illustrated as shown in Figure 2. The tools move together in the feed direction. The tool that cuts the workpiece first is numbered as tool 1. Cutting depths of each tool can be different; the cutting depth of tool 1 and tool 2 are represented by a_1 and a_2, respectively. In order to keep the stability formulation in one dimension [9] and focus more on the effects of parallel machining, the tools are considered to have no side cutting edge and oblique angles. In this case, only the displacements of the tools in the feed direction affect the regeneration mechanism. Each tool can be modeled as being attached to a rigid surface of the machine with springs (k_1,k_2) and damping elements (b_1,b_2) as shown in Figure 2. Moreover, there is dynamic interaction between the cutting tools which is represented by spring and damping elements (k_{12} and b_{12}) . Due to this interaction, the process is dynamically parallel, i.e., the dynamic cutting force on each tool affects the dynamic displacement of the other. The dynamics of the workpiece can easily be included in the formulation. However, it is neglected here since the workpiece is considerably rigid with respect to the cutting tools along its longitudinal axis, i.e., the Z–axis.

For the stability analysis, the dynamic chip thickness of each cutting tool is formulated first. The feed per revolution values (h_o) of both tools are the same since they move together on the same turret. As shown in Figure 2, dynamic displacements on the tools occur due to forces (F_1, F_2) in the feed direction. The displacements of tool 1 and tool 2 are represented by z_1 and z_2, respectively. Dynamic chip thicknesses (h_1, h_2) of each tool resulting from the dynamic displacements are expressed as:

$$\begin{aligned} h_1(t) &= h_o - z_1(t) + z_1(t-\tau) \\ h_2(t) &= h_o - z_2(t) + z_2(t-\tau) \end{aligned} \quad (1)$$

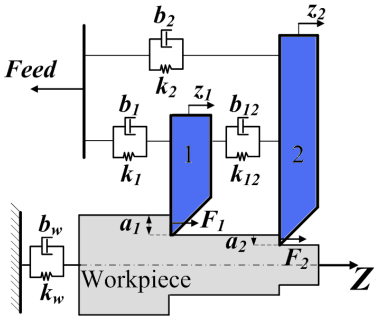

Figure 2: Parallel turning on different surfaces

where τ is rotation period of the workpiece in seconds, and t represents the present time. The dynamic chip thicknesses are affected by the dynamic displacements between two sequential rotation periods. Since the static chip thickness, h_o, does not affect the regeneration mechanism [12], it can be excluded from the stability formulation. The dynamic displacements can be expressed by transfer functions of the system and dynamic cutting forces as shown below:

$$\begin{bmatrix} z_1(t) \\ z_2(t) \end{bmatrix} = \begin{bmatrix} G_{11} & G_{12} \\ G_{21} & G_{22} \end{bmatrix} \begin{bmatrix} F_1(t) \\ F_2(t) \end{bmatrix} \quad (2)$$

where G_{ij} is the transfer function that represents the dynamics of the i^{th} tool in response to a force generated by the j^{th} tool. These transfer functions can be measured by tap-testing and modal analysis [12]. Dynamic forces in the feed direction are expressed in terms of the feed cutting force coefficient, K_f, cutting depths and the dynamic chip thicknesses as follow:

$$\begin{bmatrix} F_1(t) \\ F_2(t) \end{bmatrix} = \begin{bmatrix} K_f a_1 h_1(t) \\ K_f a_2 h_2(t) \end{bmatrix} \quad (3)$$

As can be seen from the above relation, edge forces are neglected in the stability analysis since they do not contribute to the regenerative process. By substituting the equations for dynamic chip thickness into Eq. (3), the following equation is obtained:

$$\begin{bmatrix} F_1(t) \\ F_2(t) \end{bmatrix} = \begin{bmatrix} K_f a_1 (z_1(t-\tau) - z_1(t)) \\ K_f a_2 (z_2(t-\tau) - z_2(t)) \end{bmatrix} \quad (4)$$

The dynamic displacements and cutting forces when the system is marginally stable can be expressed as,

$$\begin{bmatrix} z_1(t) \\ z_2(t) \end{bmatrix} = \begin{bmatrix} z_1 \\ z_2 \end{bmatrix} e^{i\omega_c t}, \quad \begin{bmatrix} F_1(t) \\ F_2(t) \end{bmatrix} = \begin{bmatrix} F_1 \\ F_2 \end{bmatrix} e^{i\omega_c t} \quad (5)$$

Marginal stability refers to the transition phase between the stable region and unstable region. Since the two tools are interacting with each other dynamically, they vibrate with the same chatter frequency ω_c. Additionally, the dynamic displacement values in the previous rotation at the limit of stability can be written as follows [12]:

$$\begin{bmatrix} z_1(t-\tau) \\ z_2(t-\tau) \end{bmatrix} = \begin{bmatrix} z_1(t) \\ z_2(t) \end{bmatrix} e^{-i\omega_c \tau} \tag{6}$$

By substituting equations (2), (5) and (6), into Eq. (4), the cutting forces at the stability limit become:

$$\begin{bmatrix} F_1 \\ F_2 \end{bmatrix} e^{i\omega_c t} = K_f (e^{-i\omega_c \tau} - 1) \begin{bmatrix} a_1 & 0 \\ 0 & a_2 \end{bmatrix} \begin{bmatrix} G_{11} & G_{12} \\ G_{21} & G_{22} \end{bmatrix} \begin{bmatrix} F_1 \\ F_2 \end{bmatrix} e^{i\omega_c t} \tag{7}$$

In order to simplify the equation above, a new matrix $\boldsymbol{B}$ is defined below:

$$\boldsymbol{B} = K_f (e^{-i\omega_c \tau} - 1) \begin{bmatrix} a_1 & 0 \\ 0 & a_2 \end{bmatrix} \begin{bmatrix} G_{11} & G_{12} \\ G_{21} & G_{22} \end{bmatrix} \tag{8}$$

2.2 Two turning tools on different turrets

A parallel turning process with two turning tools on different turrets is demonstrated in Figure 3. They cut the same surface but the cutting depths of the tools can be different. According to the notation used in the model, the tool with a higher cutting depth is named as the second tool (Figure 3). The flexibilities of the tools in Z direction are considered only in this case. Since the workpiece is relatively rigid with respect to the cutting tools, the workpiece flexibility is neglected. Although there is no dynamical coupling between the tools, they are dynamically dependent since vibration waves left by each tooth on the workpiece surface affect the other tooth's dynamic chip thickness.

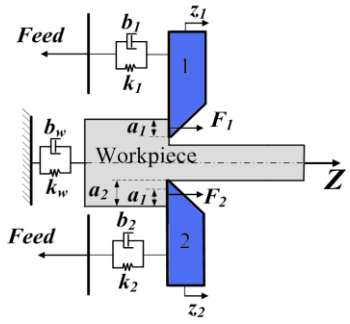

Figure 3: Parallel turning on the same surface

Due to the dynamic cutting forces on each tool (F_1 and F_2), the dynamic displacements (z_1 and z_2) develop on the tools. These displacements affect the dynamic chip thickness values, and the dynamic cutting forces on each tool can be written as follows:

$$\begin{bmatrix} F_1(t) \\ F_2(t) \end{bmatrix} = K_f \begin{bmatrix} a_1 \left(\frac{h_o}{2} - z_1(t) + z_2\left(t - \frac{\tau}{2}\right)\right) \\ a_1 \left(\frac{h_o}{2} - z_2(t) + z_1\left(t - \frac{\tau}{2}\right)\right) + (a_2 - a_1)(h_o - z_2(t) + z_2(t-\tau)) \end{bmatrix} \tag{9}$$

Unless the cutting depths on each tool are equal, there are two different regions with different mechanical and dynamic characteristics in the process. The region with depth of a_1 is removed by both of the tools. In this region, dynamic chip thickness on a tool is affected by the displacement of the tool at present time and the displacement of the other tool at a half rotation period ($\tau/2$) before. The feed per revolution h_o is shared between the tools in this region as the static chip thickness. On the other hand, the region with a depth of a_2-a_1 is only removed by the second tool. Hence, the dynamic chip thickness depends on the dynamic displacement of the second tool at present time and at one rotational period (τ) before. The static chip thickness on the second tool is equal to the feed per revolution in this region.

Since the static chip thicknesses on the tools do not affect the regeneration mechanism, they can be removed from the formulation presented in Eq. (9) for stability analysis. Dynamic displacements (z_1 and z_2) can be calculated in terms of cutting forces and transfer functions as follows:

$$\begin{bmatrix} z_1(t) \\ z_2(t) \end{bmatrix} = \begin{bmatrix} G_{11} F_1(t) \\ G_{22} F_2(t) \end{bmatrix} \tag{10}$$

Dynamic displacements and dynamic cutting forces on the tools at the limit of the stability can be written using Eq.(5). Dynamic displacement of the second tool one rotational period before can be determined using Eq. (6). Moreover, the displacements one half of the rotation period before can be calculated using the following formulation:

$$\begin{bmatrix} z_1\left(t - \frac{\tau}{2}\right) \\ z_2\left(t - \frac{\tau}{2}\right) \end{bmatrix} = \begin{bmatrix} z_1(t) \\ z_2(t) \end{bmatrix} e^{-i\omega_c \frac{\tau}{2}} \tag{11}$$

After the presented formulations are substituted into Eq. (9) and re-arranged, the cutting forces at the limit of stability can be written as follows:

$$\begin{bmatrix} F_1 \\ F_2 \end{bmatrix} e^{i\omega_c t} = \boldsymbol{B} \begin{bmatrix} F_1 \\ F_2 \end{bmatrix} e^{i\omega_c t} \tag{12}$$

where $\boldsymbol{B}$ matrix for this case is presented below:

$$\boldsymbol{B} = K_f \begin{bmatrix} -a_1 G_{11} & a_1 G_{22} e^{-i\omega_c \frac{\tau}{2}} \\ a_1 G_{11} e^{-i\omega_c \frac{\tau}{2}} & a_2 G_{22}(e^{-i\omega_c \tau} - 1) - a_1 G_{22} e^{-i\omega_c \tau} \end{bmatrix} \tag{13}$$

3. Calculation of stability diagrams

The procedure for generation of stability diagrams for the two cases considered is presented in this section. After some arrangements, the relations developed for dynamic cutting forces in Eq. (7) and Eq. (12) take the following form:

$$[\boldsymbol{I} - \boldsymbol{B}] \begin{bmatrix} F_1 \\ F_2 \end{bmatrix} = 0 \tag{14}$$

where I is the 2*2 identity matrix. In order to have non-trivial solutions at the stability limit, the determinant of [$\boldsymbol{I}$-$\boldsymbol{B}$] matrix should be equal to zero. The determinant results in a complex equation with variables a_1, a_2, ω_c and τ. When the real and imaginary parts of the equation are grouped and equated to zero, two independent equations are obtained (Eq. (15)) [12]. Since the resulting equations are lengthy, they are presented symbolically as follows:

$$\begin{aligned} \text{Real}(\det[\boldsymbol{I}-\boldsymbol{B}]) &= 0 \\ \text{Imag}(\det[\boldsymbol{I}-\boldsymbol{B}]) &= 0 \end{aligned} \quad (15)$$

In the first parallel turning case presented in section 2.1, the cutting depth a_2 is the height difference between tip positions of tool 1 and tool 2. It is set after the tools are fixed on the tool holder. For that reason, a_2 is a known parameter for a given configuration. Thus, the stability diagram for a_1 can be determined for a given a_2.

For the second parallel turning case explained in the section 2.2, the cutting depth on the second tool, a_2, should be selected before the stability analysis. Similar to the first case, the stability diagram for a_1 can be obtained for a given a_2. But it should be remembered that that a_2 is selected as higher than a_1 in the related formulation. Hence, only the stability limit values for a_1 which are less than a_2 should be considered as solution

After these explanations, there are three unknowns, namely a_1, ω_c and τ, in the formulation for both parallel turning cases whereas there are only two independent equations at hand. Cutting depth a_1 is solved in terms of ω_c and τ using the real part of the complex equation in Eq. (15) and this relation is substituted into the imaginary part of the complex equation in Eq. (15). Hence, a_1 term is eliminated, and the imaginary part of the complex equation is obtained with 2 parameters, ω_c and τ, only. The resulting equation includes many trigonometric functions, and thus a closed form analytical solution for ω_c or τ is not possible to obtain. Hence, a search algorithm, named as golden section search [13], is used to solve τ for a given ω_c.

In the solution procedure, firstly a chatter frequency range is selected where $\omega_{c,min}$, $\omega_{c,max}$ and $\Delta\omega$ represent lower limit, upper limit and increment of the frequency range, respectively. Since chatter frequencies (ω_c) are expected to be close to the natural frequency of the tools, the selected range should contain all the natural frequencies of the system. Then, the spindle speeds are swept with Δn increments for a given chatter frequency (ω_c). Each spindle speed n corresponds to a rotational period τ by $n=60/\tau$. For each ω_c and τ pair, the imaginary part of the complex equation in Eq. (15) is calculated. If there is a sign change between consecutive τ values, a root of the equation is bracketed in an interval with a width of Δn. Then, using the golden section search [13], spindle speed value that satisfies the equation is identified with a preset tolerance. For each chatter frequency, more than one spindle speed is determined corresponding to different lobe numbers in the stability diagram. Using calculated rotational periods and given chatter frequencies, a_1 values are calculated by the real part of the Eq. (15). ω_c and τ pairs resulting in negative a_1 values are eliminated from the solutions. Finally, the stability diagram can be obtained by plotting a_1 with respect to the spindle speed. Since a search algorithm is employed to obtain the stability diagrams, increments in the frequency and spindle speed ranges, which are represented by $\Delta\omega$ and Δn, have considerable effects on the stability diagrams. Hence, they should be selected small enough until a convergence in the solution is obtained.

4. Experimental Results and Simulations

In the tests, 1050 steel work material and TPGN 160304 TT1500 cutting inserts are used. For feed values between 0.005mm and 0.13mm and cutting speed of 200 m/min, the edge and cutting force coefficients in the feed direction are calibrated as 116N/mm and 872 MPa, respectively, using the linear-edge force model[14].

The FRFs of the flexible structures are measured using tap testing as shown in Figure 4. The modal data is determined using Cutpro software [15] and the transfer functions are calculated using the following equation:

$$G_{ik}(j\omega) = \sum_{r=1}^{q} \frac{1/m_r}{(j\omega)^2 + 2\xi_r\omega_{n,r}(j\omega) + {\omega_{n,r}}^2} \quad (16)$$

where q is the number of modes used to represent the transfer function. The stability results for two different examples that represent the two processes explained in section 2 are presented here. In the first example, a standard turning machine tool (Mori Seiki NL 1500) is used with a special tool holder, and in the second example a parallel machine tool (Index ABC) is employed.

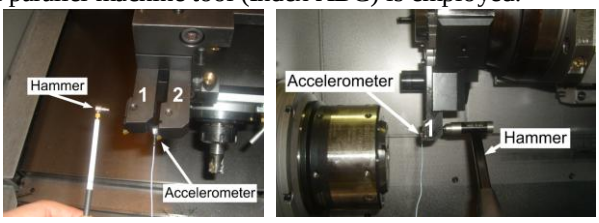

(a) (b)

Figure 4: Measurement of FRFs for different processes

4.1 The first example

In this example, the cutting tools are clamped on the same turret with a special tool holder in order to achieve parallel turning process on a standard turning machine (Figure 4(a)). Due to the design of the tool holder, cutting depth of the second tool a_2 is fixed after the tools are clamped to the holder. Second tool is clamped in such a way that a_2 becomes 4.7mm in the parallel turning operation. The modal data determined for the tools are tabulated in Table 1. The workpiece is an 85 mm diameter cylinder (Figure 1(a)) and it's relatively rigid with respect to the tools in the feed direction.

First of all, using the orthogonal stability model [12], the stability diagram for each tool is calculated for independent operation. The absolute stability limits of the first and second tools are around 4.45 mm 5.45mm, respectively. The chatter frequencies that result in the minimum stability are quite different on each tool. The chatter frequency at the absolute stability for the first tool is 2325Hz whereas for the second tool it is 3680 Hz.

The stability diagram for a_1 when two tools work in parallel is presented in Figure 5. The first tool's absolute stability limit decreases slightly due to the second tool. But comparing this decrease with the additional depth of cut of 4.7 mm removed by the second tool, it can be claimed that parallel turning is very advantageous as the total stable material removal rate nearly doubles compared to the case with only one tool is in cut.

	Mode	f_n(Hz)	ζ(%)	k(N/m)
G_{11}	1	2086.1	5.71	$4.875*10^7$
	2	2290.7	1.61	$2.272*10^8$
	3	3899.9	1.22	$3.591*10^8$
$G_{12}=G_{21}$	1	2067.1	5.55	$1.635*10^8$
	2	3572.7	5.35	$-2.189*10^8$
G_{22}	1	2050.7	4.78	$6.753*10^8$
	2	2553.9	2.87	$8.602*10^8$
	3	3036.1	6.09	$5.903*10^7$
	4	3443.5	1.29	$3.141*10^8$
	5	3629.6	1.61	$3.069*10^8$

Table 1: Modal data of the first example

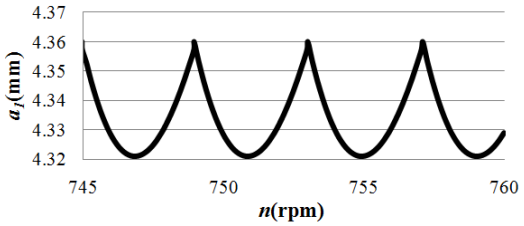

Figure 5: Stability diagram for the parallel operation, a_2=4.7mm

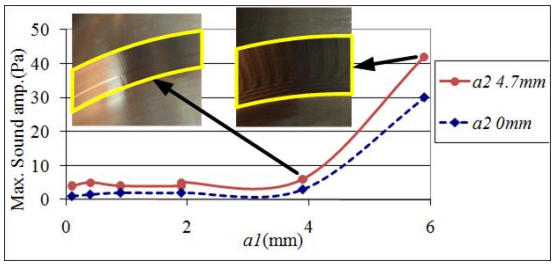

Figure 6: Variation of sound amplitude with a_1.

In order to verify the predictions, several cutting tests have been performed for single and parallel processes at 750 rpm. In both processes, the first tool's cutting depth a_1 was changed at 6 levels between 0.1 mm and 5.9 mm. During the tests, the sound amplitude was measured using a microphone that is fixed to the turret. Maximum sound amplitude is plotted with respect to cutting depth a_1 for both single and parallel processes in Figure 6. It can be seen that there is a sharp increase in sound amplitudes between a_1=3.9 mm and a_1=5.9 mm for both single and parallel processes which means that the stability limit for both cases is between 3.9 and 5.9 mm. Moreover, two photos of the surfaces created by the first tool in parallel operation are presented in Figure 6. The one on the right (a_1=5.9 mm) has chatter marks while they are not seen on the left one (a_1=3.9 mm). For the single tool process, similar result is also observed. As a result, it can be concluded that the model's predictions agree with the experimental results.

4.2 The second example

In this example case, the cutting tools are clamped on independent turrets on a parallel machine tool as shown in Figure 1(b). Although they are independent, they are programmed such that there is no relative motion between the cutting tools, and their Z coordinates are the same during the parallel turning process. Hence, they cut the same surface. The modal data measured for the first and second tool in the feed direction are tabulated in Table 2. Note that in this case the modal frequencies of the tools are quite close to each other which has significant consequences on the parallel cutting stability as it will be shown below. The workpiece is a 35mm diameter cylinder and its flexibility in the feed direction can be neglected compared to the flexibility of the cutting tools. For that reason, dynamic interaction between the tools occurs only through the effect of vibration waves left by each tool on the other tool.

Mode	f_n(Hz)	ζ(%)	k(N/m)
G_{11}	2238.9	3.23	$4.769*10^7$
G_{22}	2372.3	4.51	$1.166*10^8$

Table 2: Modal data of the second example

For independent operation of the cutting tools, the stability limits for the first and the second tools are calculated using the orthogonal stability model [12]. The first tool's absolute stability limit is determined as 3.4 mm at 2310Hz whereas the absolute stability limit of the second tool is calculated as 12.6 mm at 2480Hz.

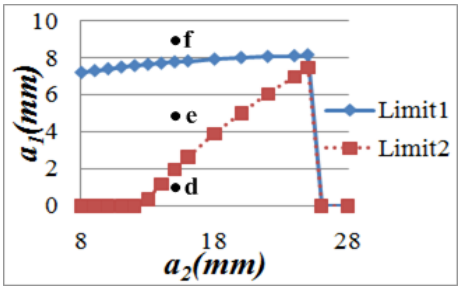

Figure 7: Effect of a_2 on absolute stability limits

When two tools work in parallel, the effect of the cutting depth a_2 on the absolute stability of the first tool is presented in Figure 7. In this case there can be two stability limits defining the boundaries of minimum and maximum stable cutting depths for the first tool. This means that the process is stable if the cutting depth is between these boundaries. This is believed to be due to very close modal frequencies of the tools which increases the dynamic interaction effects. As it was demonstrated in the previous example, parallel cutting may increase the total stability of the system due to this interaction which in this case is enhanced due to close modal frequencies. One may see this as an "absorber effect" similar to tuned vibration absorbers. The curve with legend "Limit1" in Figure 7 represents the higher absolute stability of the first tool. Note that increasing a_2 value has stabilizing effect on the system. This effect is seen for the a_2 values between 8 and 25 mm. For higher values of a_2, the process becomes unstable independent of a_1. For a_2 values higher than 12.6 mm the lower stable cutting depth, "Limit2", is also seen on the stability diagram. It also increases with a_2 and becomes closer to Limit1. For a_2 values higher than 25mm, Limit1 and Limit2 coincide and the system becomes totally unstable. In order to demonstrate the "two-limit" case, stability diagram calculated when a_2 is 25 mm is presented in Figure 8.

A time domain model is also developed for dynamics of parallel turning processes. Although its details are not

in the scope of this paper, the time domain model is used to verify the observations made in Figure 7. With that purpose, 3 points (d, e and f) are selected on Figure 7, and the variations of the displacements of first tool in time are presented in Figure 9 for spindle speed of 1825 rpm. Analyzing the trends of z_1 variations, points d and f are identified as unstable while point e is clearly a stable point. These results verify the frequency model's predictions.

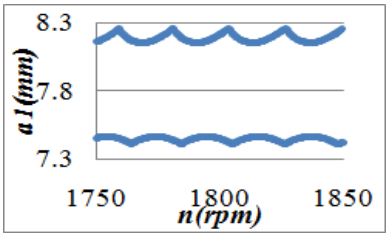

Figure 8: Stability diagram of tool 1 when a_2 is 25mm

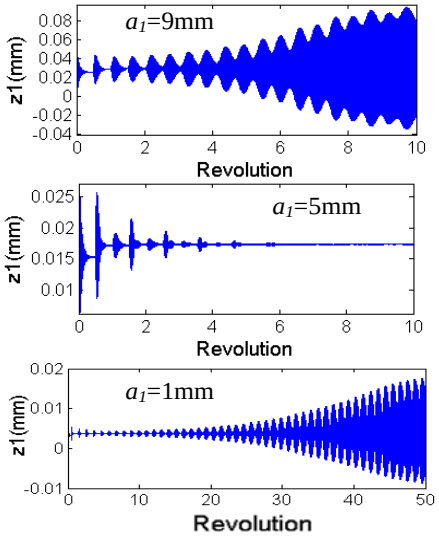

Figure 9: Variation of z_1 at points f, e, d on Figure 7.

5. Conclusion

Stability models for different parallel turning processes are presented in this paper. These models are useful for understanding the dynamic interaction of parallel working tools and predicting the effect of this interaction on stability limits. The models' results are demonstrated on several examples and advantage of parallel turning with respect to single tool turning is demonstrated. Moreover, experimental and time domain verifications of the presented models are presented. It is demonstrated that the total cutting stability in a parallel turning process can be increased compared to single tool turning due to dynamics interactions between the tools. This effect is enhanced if the modal frequencies of the tools are close to each other similar to the situation in tuned vibration absorbers.

Acknowledgement

The authors acknowledge Scientific and Technical Research Council of Turkey (TUBITAK) for its support in this research. Moreover, the authors would like thank Tankut Kocak, Ertan Guney and Gokhan Ersari from TANDEM Company for their support on the cutting tests on the Index ABC machine tool.

References

[1] Tobias, S.A. and Fishwick, W., 1958, The Chatter of Lathe Tools Under Orthogonal Cutting Conditions, Trans. of ASME, 80:1079-1088

[2] Tlusty, J., Polacek, M., 1963, The Stability of Machine Tools Against Self Excited Vibrations in Machining, Int. Research in Production Engineering, ASME, 465-474.

[3] Tlusty, J. and Ismail, F., 1981, Basic non-linearity in machining chatter, Annals of the CIRP. 30: 21-25.

[4] Moufki, A., Devillez, A. Segreti, M., Dudzinski, D., (2006) A semi-analytical model of non-linear vibrations in orthogonal cutting and experimental validation, Int. Journal of Machine Tools & Manufacture, 46 436–449

[5] Chen, C. K., Tsao, Y. M., 2006, A stability analysis of turning a tailstock supported flexible workpiece, International Journal of Machine Tools & Manufacture, 46, 18-25.

[6] Vela-Martinez, L., Jauregui-Correaa, , J. C., Rubio-Cerda, E., Herrera-Ruiz, G., Lozano-Guzman, A. 2008, Analysis of compliance between the cutting tool and the workpiece on the stability of a turning process, International Journal of Machine Tools & Manufacture, 48,1054–1062

[7] Rao, B. C. , Shin, Y. C. , 1999, A comprehensive dynamic cutting force model for chatter prediction in turning, International Journal of Machine Tools & Manufacture, 39, 1631-1654

[8] Ozlu, E., Budak, E., 2007, Analytical Modeling of Chatter Stability in Turning and Boring Operations-Part I: Model Development J. Manuf. Sci. Eng. 129, 726.

[9] Ozlu, E., Budak, E., 2007, Comparison of one-dimensional and multi-dimensional models in stability analysis of turning operations, Int. Journal of Machine Tools & Manufacture, 47, 1875–1883.

[10] Lazoglu, I., Vogler, M., Kapoor, S.G., DeVor, R.E, 1998, Dynamics of the Simultaneous Turning Process, Transactions of the North American Manufacturing Research Conference, NAMRC XXVI, pp. 135-140

[11] Ozdoganlar, O. B., Endres, W. J., 1999, Parallel-Process (Simultaneous) Machining and Its Stability, presented at ASME IMECE'99, Nashville, TN; and in Proc., Symp. on Mach. Sci. and Tech., MED-10, 361-368.

[12] Altintas Y. (2000), Manufacturing Automation: Metal Cutting Mechanics, Machine Tool Vibrations and CNC Design, Cambridge University Press.

[13] Press, W.H., Teukolsky, S. A., Vetterling, W. T., Flannery, B. P., 2002, Numerical Recipes in C++: The Art of Scientific Computing, Cambridge University Press.

[14] Budak, E., Altintas, Y., Armarego, E.J.A., 1996, Prediction of milling force coefficients from orthogonal cutting data, Transactions of the ASME Journal of Manufacturing Science and Engineering 118, 216–224.

[15] Cutpro: www.malinc.com